Applied Catalysis B: Environmental 330 (2023) 122659

Contents lists available at ScienceDirect

Applied Catalysis B: Environmental

journal homepage: www.elsevier.com/locate/apcatb

Porous graphitized carbon-supported FeOCl as a bifunctional adsorbent-catalyst for the wet peroxide oxidation of chlorinated volatile organic compounds: Effect of mesopores and mechanistic study

Cong Pan [a], Wenyu Wang [a], Yihui Zhang [a], Jong Chol Nam [a], Feng Wu [a], Zhixiong You [a], Jing Xu [b,*], Jinjun Li [a,*]

[a] School of Resource and Environmental Sciences, Hubei Key Lab of Bioresource and Environmental Biotechnology, Wuhan University, Wuhan 430079, China
[b] State Key Laboratory of Water Resources and Hydropower Engineering Science, Wuhan University, Wuhan 430072, China

ARTICLE INFO

Keywords:
CVOCs
Iron oxychloride
PGC
Wet scrubber
Catalytic wet peroxide oxidation

ABSTRACT

Wet scrubbing coupled with adsorption-enhanced heterogeneous advanced oxidation processes (AOPs) are promising approaches to the treatment of chlorinated volatile organic compounds (CVOCs). However, microporous activated carbon-based adsorbents and catalyst supports have the disadvantage of difficult molecule diffusion. Herein, we have demonstrated that porous graphitized carbon (PGC) allowed faster intra-particle diffusion of organic molecules due to its well-developed mesoporous structure. Therefore, a wet scrubbing system containing H_2O_2 and a PGC-supported FeOCl catalyst has been developed to effectively remove gaseous dichloroethane, trichloroethylene, dichloromethane and chlorobenzene. The scrubber performed well at pH 3.0 using a FeOCl/PGC dosage of 0.2 g/L and initial H_2O_2 concentration of 40 mM. Its good long-term performance was achieved by replenishing H_2O_2 to maintain a suitable concentration. The degradation pathways of dichloroethane have been proposed using a combination of intermediate analysis and density functional theory calculations. PGC-supported catalysts may be desirable bifunctional adsorbent-catalyst materials for wet scrubbing of CVOCs.

1. Introduction

Volatile organic compounds (VOCs) are the main precursors of photochemical smog and secondary organic aerosols, which pose a great threat to human health and the environment [1–4]. In particular, chlorinated volatile organic compounds (CVOCs) emitted by chemical, electroplating, ceramics and other industries are often toxic or carcinogenic, and difficult to treat [5–7]. Some technologies, such as catalytic combustion, photocatalytic oxidation and incineration, have been developed to destroy CVOCs [8–11]. However, these technologies have disadvantages, including high energy consumption, facile catalyst deactivation, and the generation of more toxic secondary pollutants. Although adsorption and condensation are considered as economical and convenient methods used to eliminate VOCs, they cannot degrade and mineralize VOCs and require post-treatment processing [12,13].

The wet chemical scrubbing process has the advantages of simple operation, mild reaction conditions and low cost, and has been used to treat low-concentration VOCs [13,14]. It involves the mass transfer of VOCs from air to water, and their subsequent reaction with dissolved oxidants, such as NaClO and peroxymonosulfate. However, the oxidant alone often reacts slowly with VOCs, leading to a poor removal efficiency. In addition, toxic by-products may be produced, such as ClO_2 [15,16]. To address these issues, researchers have developed wet scrubbing systems coupled with advanced oxidation processes (AOPs) [17–20]. The basic idea is to activate the oxidant, such as H_2O_2 and persulfates, to generate $HO^{\bullet}$, $SO_4^{\bullet-}$ and other reactive oxygen species, which can rapidly and efficiently oxidize organic molecules, even recalcitrant chlorinated organic compounds [21,22].

Abbreviations: AC, activated carbon; AOPs, advanced oxidation processes; BA, benzoic acid; CB, chlorobenzene; CVOCs, chlorinated volatile organic compounds; DCE, 1,2-dichloroethane; DCM, dichloromethane; DFT, density functional theory; DMPO, 5-Dimethyl-1-pyrroline-N-oxide; ESR, electron spin resonance; MeOH, methanol; NPA, natural population analysis; PGC, porous graphitized carbon; PMSO, methyl phenyl sulfoxide; $PMSO_2$, methyl phenyl sulfone; TBA, tert-butyl alcohol; TCE, trichloroethylene; TEMP, tetramethylpiperidine; TOC, total organic carbon.

* Corresponding authors.
E-mail addresses: jingxu0506@whu.edu.cn (J. Xu), lijinjun@whu.edu.cn (J. Li).

https://doi.org/10.1016/j.apcatb.2023.122659
Received 2 December 2022; Received in revised form 22 February 2023; Accepted 17 March 2023
Available online 20 March 2023

The homogeneous Fenton system (Fe^{2+}/H_2O_2) has been used to degrade VOCs [23,24],which involves the generation of $HO^{\bullet}$ as the primary oxidizing species (Eq. (1)) and $^{\bullet}O_2H$ as the secondary oxidizing species (Eq. (2)). However, the reduction of the generated Fe^{3+} species into Fe^{2+} (Eq. (3)) is significantly slower than the consumption of Fe^{2+} (Eq. (2)), which severely limits the continuous generation of $HO^{\bullet}$ [24]. Moreover, iron hydroxide sludge, which accumulates in the system (Eq. (4)), causes secondary pollution [25]. Alternatively, heterogeneous Fenton-like processes using solid catalysts such as nano-zero-valent iron [26], iron oxide [27–29] and goethite [30] to activate H_2O_2 avoid the generation of iron hydroxide sludge. However, they generally show lower catalytic activity than the homogeneous Fenton process. FeOCl is a type of layered metal oxyhalide, which can more effectively activate H_2O_2 to degrade pollutants than other heterogeneous iron-based catalysts due to its distinctive Fe-O-Fe and O-Fe-Cl linear structure, and the unsaturated iron atoms exposed on its surface [31,32]. This special coordination environment promotes the conversion of Fe^{3+} into Fe^{2+}, realizing the Fe^{2+}/Fe^{3+} cycle and continuous activation of H_2O_2 [33,34].

$$Fe^{2+} + H_2O_2 \rightarrow Fe^{3+} + OH^- + HO^{\bullet} \quad k_1 = 40\text{–}80\ L{\bullet}mol^{-1}{\bullet}s^{-1} \tag{1}$$

$$Fe^{3+} + H_2O_2 \rightarrow Fe^{2+} + {}^{\bullet}O_2H + H^+ \quad k_2 = 9{\cdot}1 \times 10^{-7}\ L{\bullet}mol^{-1}{\bullet}s^{-1} \tag{2}$$

$$Fe^{3+} + {}^{\bullet}O_2H \rightarrow Fe^{2+} + O_2 + H^+ \quad k_3 = 0{\cdot}33\text{–}2{\cdot}1 \times 10^{-6}\ L{\bullet}mol^{-1}{\bullet}s^{-1} \tag{3}$$

$$Fe^{3+} + 3OH^- \rightarrow Fe(OH)_3\downarrow \tag{4}$$

Another key factor limiting the efficiency of the wet scrubbing of organic waste gases is the poor water solubility of many VOCs, which makes air-water mass transfer difficult. Very recently, we used a wet scrubbing system containing H_2O_2 and activated carbon (AC)-supported iron oxychloride (FeOCl) to remove airborne dichloroethane (DCE) [35], in which DCE was concentrated on AC via adsorption, facilitating its reaction with $HO^{\bullet}$ generated through the activation of H_2O_2 by FeOCl. In the presence of H_2O_2, the Fe^{2+}/Fe^{3+} cycle on FeOCl enables the continuous production of $HO^{\bullet}$. However, ACs are generally microporous, which can result in difficult diffusion during the adsorption of VOCs, although the micropores have a strong adsorption force on the captured molecules [36–38]. In particular, this effect may be more pronounced in water than in air, as the former is much more viscous. Therefore, the diffusion rate of organic matter in water is slower. We have prepared porous graphitized carbons (PGCs) with mesoporous structures using a KOH-promoted catalytic graphitization method, which allows enhanced adsorption kinetics in the dynamic adsorption of airborne VOCs [38–40].

In this study, we aimed to develop a PGC-supported FeOCl catalyst for use in the wet scrubbing of various CVOCs and to establish the relationship between the mesoporosity of PGC and efficiency of the scrubbing system. The main reactive oxygen species in the wet scrubbing system were identified using electron spin resonance (ESR) spectroscopy and free radical probe experiments, and the degradation mechanism was studied using product analysis. This study can provide some fundamental insights into the treatment of CVOCs by FeOCl-based Fenton-like systems.

2. Materials and methods

2.1. Materials and methods

Commercial AC, $FeCl_3{\bullet}6\ H_2O$, $NiCl_2{\bullet}6\ H_2O$, ethylenediamine (EDA), H_2O_2 (30%), KOH, potassium titanium oxalate, concentrated H_2SO_4 (95.0–98.0%), 1,2-dichloroethane (DCE), trichloroethylene (TCE), chlorobenzene (CB), dichloromethane (DCM), tert-butyl alcohol (TBA) and methanol (MeOH) were purchased from Sinopharm Chemical Reagent Company Limited (Shanghai, China). Methyl phenyl sulfoxide (PMSO), methyl phenyl sulfone ($PMSO_2$), benzoic acid (BA), Na_2CO_3, $NaHCO_3$, tetramethylpiperidine (TEMP) and 5, 5-Dimethyl-1-pyrroline-N-oxide (DMPO) were obtained from Aladdin Technology Company Limited (Shanghai, China). Unless otherwise specified, all the chemicals were of analytical grade and used as received. Tap water was obtained from Wuhan University. The main parameters of deionized water and tap water are listed in Table S1.

2.2. Material preparation

2.2.1. Synthesis of PGCs

The PGCs were prepared by the KOH-promoted catalytic graphitization method reported recently with minor modifications [38–40]. Typically, 2.85 g of $NiCl_2{\bullet}6\ H_2O$ was dissolved in 30 mL of deionized water, then 4.0 mL of EDA was slowly added. Under continuous stirring, 6.0 g of KOH was added to form a clear solution, followed by 3.0 g of AC. The mixture was transferred to a hot plate to evaporate the water. Afterward, the solid was transferred to a corundum boat and inserted into a tubular corundum reactor located in an electrical furnace. Under 110 mL/min of N_2 flow (25 ℃ and 1 atm), the solid was ramped up to 250 °C at a heating rate of 10 °C/min and held for 1 h, and then ramped to 900 °C and held for 2 h. After cooling, the solid was washed with aqueous HCl (15%) and deionized water to remove Ni and KOH. Finally, the sample was dried at 100 °C to obtain a product named PGC4, where the number 4 indicated the ratio of Ni to AC (mmol/g) in the preparation. In the same way, PGC0, PGC1, PGC3 and PGC8 were also prepared. Without the use of Ni catalyst, PGC0 was actually a further activated AC.

2.2.2. Synthesis of FeOCl/PGC

FeOCl supported on PGC was prepared by a thermal transformation of impregnated $FeCl_3{\bullet}6\ H_2O$, as reported recently with minor modifications [41]. In a typical synthesis, 0.5 g of $FeCl_3{\bullet}6\ H_2O$ was dissolved in 7.0 mL of deionized water and slowly dropped onto 1.8 g of PGC. After mixing well, the mixture was aged at room temperature for 24 h, and then transferred to a tubular furnace and heated at 150 °C for 2 h under N_2 flow. After cooling, the solid was washed with ethanol and then dried at 100 °C. The obtained product was named as 10% FeOCl/PGC, where 10% indicated the nominal weight percentage of FeOCl in the catalyst. The actual FeOCl loading was determined to be 9.3 wt% by an Avio 200 inductively coupled plasma-optical emission spectroscopy (PerkinElmer, USA). FeOCl/PGC4 catalysts with other FeOCl loadings were also prepared by adjusting the amount of $FeCl_3{\bullet}6\ H_2O$. Hereafter, unless otherwise stated, FeOCl/PGC4 refers to the catalyst with a nominal FeOCl loading of 10 wt%. An unsupported FeOCl catalyst was prepared by thermal conversion of $FeCl_3{\bullet}6\ H_2O$ at 220 °C for 2 h in N_2 flow, and the obtained powder was washed with ethanol.

2.3. Wet scrubbing experiment

A jacketed cylindrical glass reactor with an inner diameter of 8.5 cm and height of 32.0 cm was used as the wet scrubber (Fig. S1). The top of the reactor was sealed with a Teflon plug, two separate holes were used for the gas inlet and outlet, and the gas inlet pipe reached the lower part of the reactor and ended with a sand core bubbler.

In a typical wet scrubbing experiment for gaseous DCE, 1000 mL of the working solution containing 0.2 g of FeOCl/PGC was adjusted to a preset initial pH value (pH_0) using H_2SO_4 or NaOH, and then poured into the wet scrubber. DCE vapor was generated by injecting its liquid into a preheated vaporization chamber set at 110 °C in a rate-controlled manner using a TJ-1A micro-injection pump (Longer Precision Pump Company, China) and was delivered to the wet scrubbing solution via a continuous flow of N_2 gas (110 mL/min, 25 °C, 1 atm) via a sand core bubbler. A certain volume of H_2O_2 was added to initiate the reaction and magnetic stirring was continued throughout the process. The inlet and outlet concentrations of DCE were measured using an online GC-7806 gas chromatograph (Wenling Instruments, China). The removal efficiency (R) of DCE was calculated using Eq. (5):

$$R = \frac{[DCE]_{inlet} - [DCE]_{outlet}}{[DCE]_{inlet}} \times 100\% \quad (5)$$

where $[DCE]_{inlet}$ and $[DCE]_{outlet}$ are concentration of DCE at the inlet and outlet, respectively.

The concentrations of H_2O_2 in the scrubbing solution were determined using potassium titanium(IV) oxalate spectrophotometry [42]. The ESR signals were measured on an EMX nano ESR spectrometer (Bruker, Germany). PMSO was used as a probe to identify the Fe(IV) species. The concentrations of the intermediates were measured using IC-2010 ion chromatography (TOSOH, Japan). The dissolved Fe(II) and Fe(III) ions were measured using the 1,10-phenanthroline method [43]. Details of the analytical methods used in this study are presented in Text S1 and S2.

2.4. Characterization

Nitrogen adsorption-desorption isotherms were acquired on a V-Sorb 2800 P surface area and porosimetry analyzer (Gold APP, China). The specific surface areas were calculated based on the Brunauer-Emmett-Teller (BET) equation. The pore size distributions (PSDs) were derived from the adsorption branches of the isotherms through the non-local density functional theory (NLDFT) model, using SAIEUS program (Free Version 2.0). X-ray diffraction (XRD) patterns were acquired using an Miniflex600 X-ray diffractometer (Rigaku, Japan), with Cu-Kα radiation. Microscopic images and morphologies of the materials were obtained by a JEM-2100 transmission electron microscopy (TEM) (JEOL, Japan) and a MIRA 3 LMH scanning electron microscopy (SEM) (TESCAN, Czech Republic). The graphitization degree of PGC and FeOCl/PGC was identified by a Raman DXR spectrometer (Thermo, USA) with a 532 nm laser. Catalyst surface elements were analyzed by an ESCALAB 250Xi X-ray photoelectron spectroscopy (XPS) (Thermo, USA) with Al-Kα radiation.

3. Results and discussion

3.1. Material characterization

The crystal structures of the materials were observed using XRD. The PGCs exhibit the well-defined structures of graphitized carbon, and increasing the Ni/C ratio during the synthesis results in an increased degree of graphitization in the products (Fig. S2a). The XRD pattern obtained for the unsupported FeOCl (Fig. 1a) match well with the orthorhombic phase (PDF #24–1105) [34,44]. Weak FeOCl diffraction peaks were observed in 50% FeOCl/PGC4. The diffraction became insignificant upon decreasing the FeOCl content.

Fig. 1b and c show the TEM images of PGC4 and FeOCl/PGC4, respectively. PGC4 was composed of flakes and hexagonal particles with sizes of ~100 nm appear on the flakes of FeOCl/PGC4. The selected area electron diffraction (SAED) pattern of the particles shows diffraction rings that match well with the (010), (110) and (021) planes of orthorhombic FeOCl (Fig. 1c insert), which was in agreement with the XRD pattern (Fig. 1a).

The N_2 adsorption-desorption isotherms of the PGCs and FeOCl/PGCs are shown in Figs. S2b and 1d, respectively. The majority of the N_2 uptake by PGC0 and FeOCl/PGC0 occurs at a low relative pressure of < 0.1 and the isotherms are overall of type *I*, which is typical for dominantly microporous ACs [45]. In contrast, N_2 adsorption on other PGCs and FeOCl/PGCs continues to increase with relative pressure and all of the isotherms have hysteresis loops, which indicate the presence of mesopores. The PGCs typically contain few-layer graphene flakes with various sizes and the heterogeneous stacking of these flakes can easily form house-of-card structures, leading to large pores [38–40]. The isotherm features of any of the FeOCl/PGC catalysts were very similar to their corresponding PGC support with only a slight decrease in nitrogen uptake observed, which indicates that the catalyst loading did not significantly alter the porosity of the carbon material. The NLDFT PSDs show that the mesopore distribution was extended after graphitization

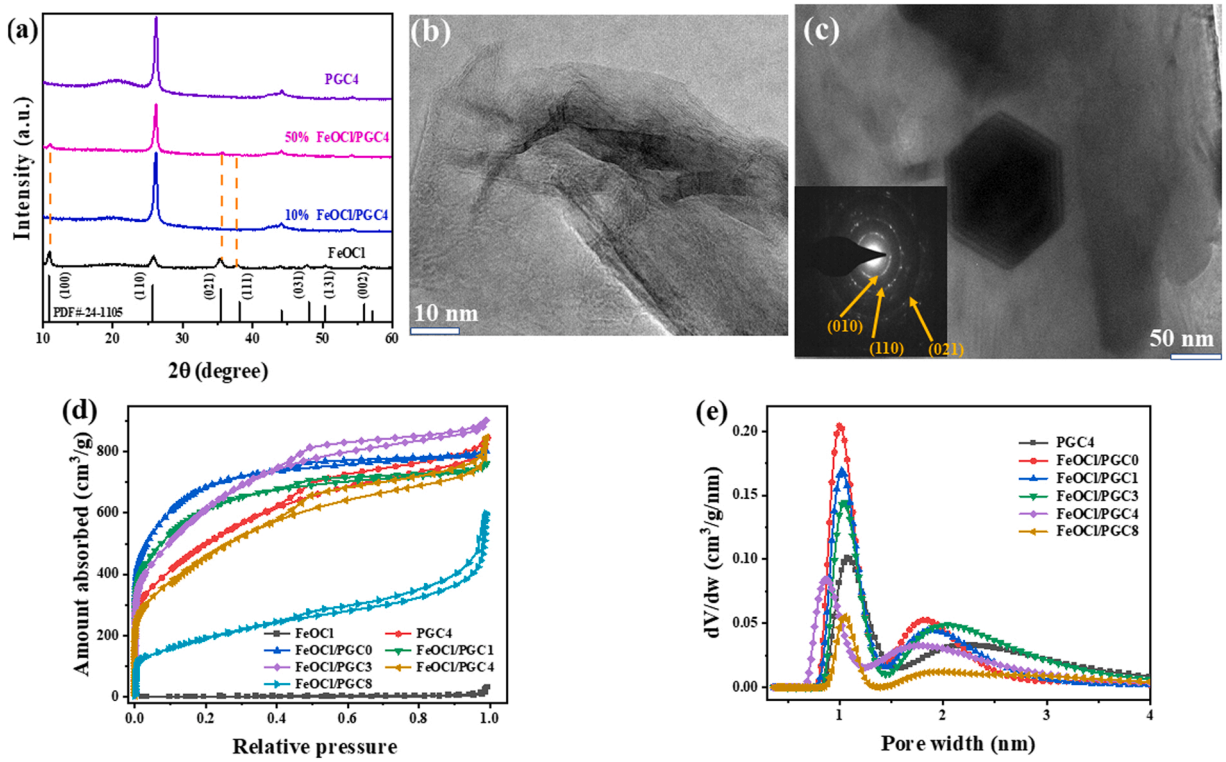

Fig. 1. (a) XRD patterns of FeOCl, PGC and FeOCl/PGC. (b and c) TEM images and SAED pattern (insert) of PGC4 and FeOCl/PGC4. (d) Nitrogen adsorption–desorption isotherms and (e) pore size distribution curves of different materials.

(Fig. 1e and S2c). The derived textural properties are shown in Table 1. The specific surface area of the carbon materials gradually decreases with an increase in the degree of graphitization. PGC0 had the smallest mesopore volume of only 0.24 cm^3/g, while PGC4 had the largest mesopore volume of 0.83 cm^3/g. The unsupported FeOCl was almost non-porous with a small specific surface area of 2 m^2/g.

3.2. Comparison of different wet scrubbing systems

As the stirring rate and gas flow rate determine the degree of mixing and contact between the CVOCs and scrubbing liquid, we investigated the effect of the stirring rate and gas flow rate on the removal efficiency of DCE in a typical wet scrubbing system comprised of FeOCl/PGC4 +H_2O_2. Increasing the stirring rate promotes the mixing of gas and the solution, promoting the removal of DCE, but when the stirring rate was increased to > 500 rpm, no significant differences in the DCE removal efficiency was observed (Fig. S3a). When the gas flow rate was < 110 mL/min, the DCE removal efficiency was relatively high (Fig. S3b). Hereafter, if not otherwise specified, the stirring rate was 500 rpm and the gas flow rate was 110 mL/min.

The performances of different wet scrubbing systems for the removal of DCE were investigated (Fig. 2a). Using pure water alone as the absorbent, the DCE removal efficiency dropped rapidly, to only 5.9% after 500 min. Using the Henry's law constant of 0.95 mol/L/atm for DCE at 25 °C [46], the equilibrium concentration of DCE in water is calculated to be 2.35 mg/L when DCE concentration in the gas phase is 25 ppmv. The total absorption of DCE by pure water is 1.78 mg/L in 500 min, as calculated from the removal curve.

Upon the addition of any carbon adsorbent to the pure water, the removal efficiency of DCE continued to decrease from the beginning, but at a lower rate than that observed in the pure water system. The DCE removal efficiencies after 500 min were 26.5%, 25.0%, 22.2%, 19.7% and 16.5% for PGC0, PGC1, PGC3, PGC4 and PGC8, respectively. The order of the DCE removal efficiencies was consistent with the order of the specific surface areas of the PGCs (Table 1). The adsorption of dissolved DCE by the carbon materials reduced its concentration in water, which promotes its transfer from gas to water. For the wet scrubbing of DCE via adsorption, the removal efficiency gradually decreases as the adsorption sites are gradually occupied and the materials with larger surface area perform better due to the higher number of available adsorption sites. The performance of the FeOCl/PGC4-only system was also studied and it was found to be slightly inferior to the PGC4-only system (Fig. S4), which could be attributed to the decrease in specific surface area after loading FeOCl (Table 1).

The DCE removal curve obtained for the system after adding only H_2O_2 to pure water was almost identical to that of the pure water system (Fig. S5), indicating that H_2O_2 can itself barely oxidize DCE. In addition, the DCE removal curve obtained for the PGC4 +H_2O_2 system was also almost identical to that of the PGC4-only system (Fig. S4), implying that the catalytic peroxide oxidation of DCE by the carbon material was negligible. In sharp contrast, the removal of DCE was significantly facilitated in the FeOCl/PGC+H_2O_2 systems with the complete removal of DCE from the flowing gas achieved within < 120 min. A DCE removal of > 95% was maintained for 210 min in the FeOCl/PGC0 +H_2O_2 and FeOCl/PGC1 +H_2O_2 systems, which was maintained for at least 300 min in any of the other FeOCl/PGC+H_2O_2 systems. After 500 min, the systems using PGC0, PGC1, PGC3, PGC4 and PGC8 as the catalyst support achieved a DCE removal of 59.5%, 61.7%, 83.3%, 89.1% and 77.9%, respectively. The total uptake of DCE by FeOCl/PGC4-only system and FeOCl/PGC4 +H_2O_2 system within 500 min as derived from the removal curves were 2.34 and 5.32 mg/L, respectively. This implies that most of the DCE captured by FeOCl/PGC4 +H_2O_2 system was oxidized.

Unlike the adsorbent-only systems, the order of the DCE removal efficiencies of the AOP systems was not in the order of the specific surface areas, but in the order of the mesopore volume of the catalyst (Table 1). This implies that the pore size of the catalyst may significantly affect the heterogeneous AOPs. During catalysis, both the adsorption of organic molecules and their diffusion to the catalytically active sites are important. As the adsorption of DCE by the carbon materials continued, the micropores of the carbons were gradually occupied and blocked, which restricts the diffusion of DCE to the FeOCl particles. In contrast, the mesopores provide wider channels for enhanced mass transfer. Consequently, FeOCl/PGC4 with the highest mesopore volume exhibits the best DCE removal efficiency, while the catalyst supported on PGC0, which was dominated by micropores, shows the worst performance.

Adsorption kinetics experiments were carried out to compare the adsorption rates of organic molecules on PGC0 and PGC4. As DCE has low solubility in water and can be easily volatilized into the air, it is difficult to perform adsorption kinetics experiments in a typical batch reactor. Therefore, we used water-soluble, non-volatile glucose as a probe. The initial glucose concentration and carbon dosage were 100 and 500 mg/L, respectively. The intra-particle diffusion model developed by Weber and Morris was used and the linear form of this model is shown in Eq. (6) [47]:

$$q_t = k_p t^{0.5} + c \quad (6)$$

where k_p ($mg/g/min^{0.5}$) is the intra-particle diffusion rate constant and c (mg/g) is the intercept, which represents the thickness of the boundary layer.

The linear plots of the model obtained for glucose adsorption on PGC0 and PGC4 are shown in Fig. 2b. There are typically three linear portions observed on the plot. The first one is external adsorption-controlled (boundary layer diffusion), followed by progressive adsorption (intra-particle diffusion-controlled), and finally equilibrium [48]. PGC4 exhibits a higher k_p value for glucose adsorption during the second stage when compared to PGC0, demonstrating that the intra-particle diffusion of glucose in micro-mesoporous PGC4 was faster than that observed in microporous PGC0. Moreover, glucose adsorption on PGC4 reaches equilibrium in 120 min, but on PGC0 it took > 220 min (Fig. S6). This also suggests PGC4 allows faster adsorption of glucose.

3.3. H_2O_2 activation mechanism

Using DMPO as a probe, ESR tests were conducted to reveal the radicals generated in the wet scrubbing systems studied. The ESR signals obtained for the different systems are shown in Fig. 3a. The H_2O_2-only system, PGC4-only system and PGC4 +H_2O_2 system do not show any ESR signals corresponding to radicals that can form adducts with DMPO. In contrast, the FeOCl/PGC4 +H_2O_2 solution shows a clear ESR signal corresponding to the DMPO-$HO^•$ adduct with an intensity of 4.68 (1:2:2:1 quarter mode, $a_N = a_H = 14.9$ G), which indicates that $HO^•$ was generated [43]. We also monitored the changes in the ESR signal of the FeOCl/PGC4 +H_2O_2 system over 500 min (Fig. 3b). A significant DMPO-$HO^•$ signal was observed throughout the process, indicating that $HO^•$ was continuously produced. The ESR signal intensity gradually weakens from 4.68 to 2.96, which can be ascribed to the gradual

Table 1
Textural properties of the materials.

Sample	BET surface area (m^2/g)	Total pore volume (cm^3/g)	Mesopore volume (cm^3/g)
PGC0	2502	1.16	0.24
FeOCl/PGC0	2442	1.11	0.22
PGC1	2457	1.29	0.49
FeOCl/PGC1	2140	1.18	0.46
PGC3	2281	1.46	0.81
FeOCl/PGC3	2180	1.40	0.79
PGC4	1820	1.31	0.83
FeOCl/PGC4	1676	1.30	0.88
PGC8	802	0.93	0.73
FeOCl/PGC8	695	0.93	0.77
FeOCl	2	0.05	0.03

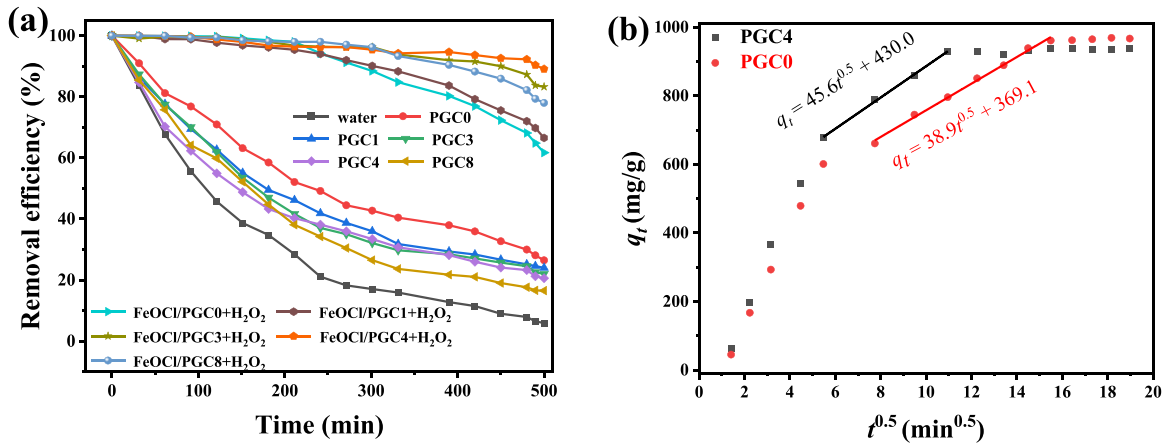

Fig. 2. (a) DCE removal efficiency in different wet-scrubbing systems and (b) intra-particle diffusion fitting curves of glucose adsorbed onto PGC0 and PGC4. Reaction conditions: $[DCE]_{inlet}$ = 25 ppmv, catalyst dosage = 0.2 g/L, $[H_2O_2]_0$ = 40 mM, pH 3.0.

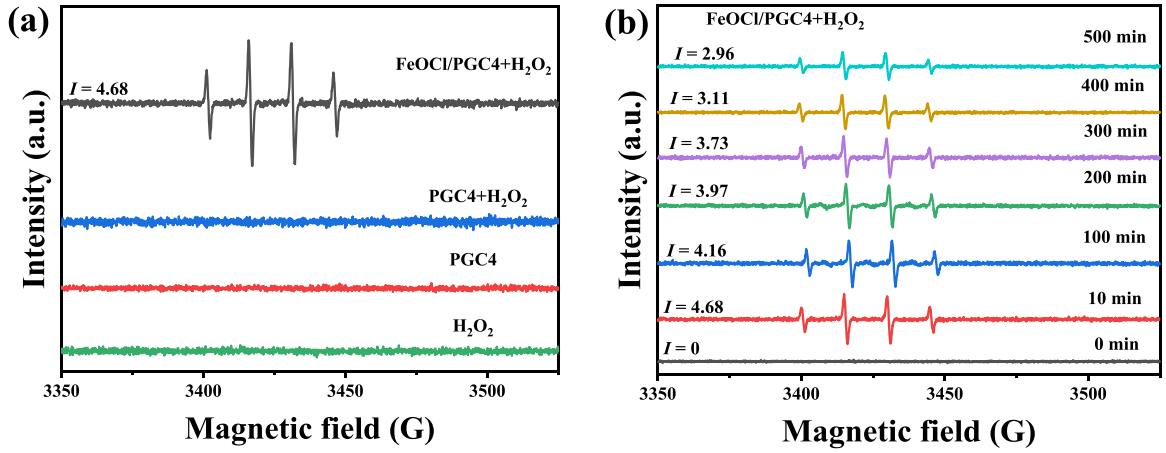

Fig. 3. (a) ESR spectra of $HO^{\bullet}$ in different systems and (b) DMPO-$HO^{\bullet}$ spectra in FeOCl/PGC4 +H_2O_2 system at different reaction times. Reaction conditions: [DMPO] = 100 mM, $[H_2O_2]_0$ = 40 mM, catalyst dosage = 0.2 g/L, pH 3.0.

depletion of H_2O_2. The H_2O_2 concentration after 500 min was < 2 mM (Fig. S7).

Previously, it has been reported that $O_2^{\bullet-}$ is also generated in the FeOCl+H_2O_2 system and $^1O_2$ could be generated via the oxidation of $O_2^{\bullet-}$ by high-valence metal ions, such as Fe^{3+} and Mo^{6+} (e.g., Eqs. (7) and (8)) [49,50]. Thus, $O_2^{\bullet-}$ and $^1O_2$ were also detected in the ESR spectra using DMPO and TEMP as probes, respectively. However, no signals attributed to the DMPO-$O_2^{\bullet-}$ and TEMP-$^1O_2$ adducts were detected (Fig. S8a-b), which suggests that $O_2^{\bullet-}$ and $^1O_2$ were not formed in the FeOCl/PGC4 +H_2O_2 system.

$$O_2^{\bullet-} + Fe^{3+} \rightarrow O_2 + Fe^{2+} \quad k_5 = 5 \times 10^7\ M^{-1}\ s^{-1} \tag{7}$$

$$Fe^{3+} + O_2^{\bullet-} \rightarrow Fe^{2+} + {}^1O_2 \tag{8}$$

Furthermore, the oxidation of FeOCl/PGC4 by H_2O_2 may produce Fe (IV) via oxygen atom transfer due to the high standard oxidation potential of H_2O_2 (1.77 V) [51]. Accordingly, methyl phenyl sulfoxide (PMSO) was used as a probe to verify the presence of Fe(IV) in the system due to the selective formation of methyl phenyl sulfoxide ($PMSO_2$) via the oxidation of PMSO by Fe(IV) [52]. Fig. S9 shows the PMSO concentration decreased by 60% over 500 min, however, $PMSO_2$ was never produced during the process. This indicates that no Fe(IV) was generated in the FeOCl/PGC4 +H_2O_2 system under the reaction conditions and the transformation of PMSO was due to its oxidation by reactive species such as $HO^{\bullet}$ [53]. Our results demonstrate that $HO^{\bullet}$ was the dominant ROS generated in the FeOCl/PGC4 +H_2O_2 system.

Scavenging experiments were performed to further evaluate the contribution of $HO^{\bullet}$ to the degradation of DCE in the FeOCl/PGC+H_2O_2 system using TBA ($k = 6 \times 10^8\ M^{-1}\ s^{-1}$) [43] and BA ($k = 5.9 \times 10^9\ M^{-1}\ s^{-1}$) [54] as $HO^{\bullet}$ scavengers. Both scavengers obviously inhibit the degradation of DCE, and the inhibitory effects were enhanced upon increasing the scavenger concentration (Fig. 4a). This confirmed that $HO^{\bullet}$ plays a vital role in the removal of DCE. This result was also confirmed using ESR experiments. Fig. 4b shows the addition of 10 mM TBA and BA decreases the DMPO-$HO^{\bullet}$ signal intensity from 4.32 to 3.56 and 2.00, respectively, and the addition of 100 mM TBA and BA further decreased the ESR signal intensity to 0.72 and 0.52, respectively.

XPS was used to analyze the surface composition and the electronic structure of the catalysts studied. The survey spectrum of FeOCl/PGC4 revealed the presence of Fe, O, Cl and C in the catalyst (Fig. 5a). The O 1 s spectrum can be deconvoluted into three components with peaks observed at 531.4, 532.5 and 533.5 eV (Fig. 5b), which were attributed to the Fe-O, Fe-OH and C=O species, respectively [34,55]. The characteristic peaks with binding energies of 198.7 and 200.3 eV can be attributed to Cl 2p (Fig. 5c) [41]. Fig. 5d shows the Fe 2p spectra of the fresh and used catalysts; the main peaks observed at 710.8 and 724.4 eV correspond to the binding energies of Fe $2p_{3/2}$ and Fe $2p_{1/2}$, respectively, and the peaks at 718.1 and 732.8 eV were satellite peaks [56]. The deconvolution of the Fe $2p_{3/2}$ spectrum revealed peaks at 710.8 and 712.6 eV, which were assigned to $Fe^{2+}$and Fe^{3+}, respectively [44,57]. The surface Fe^{2+}/Fe^{3+} ratio in the fresh catalyst was ca. 0.52, which

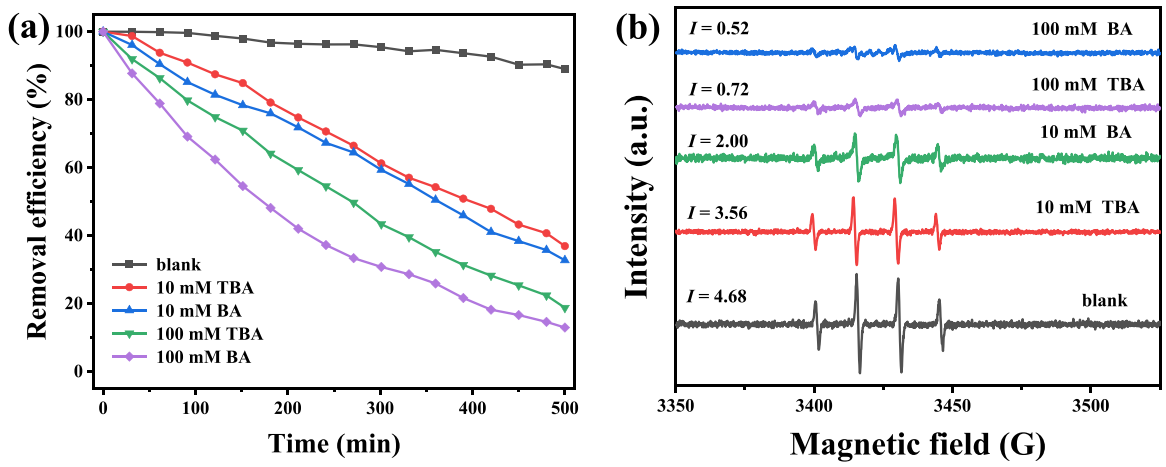

Fig. 4. (a) Effect of TBA and BA addition on DCE degradation in FeOCl/PGC4 +H_2O_2 system system;(b) ESR spectra. Reaction conditions: $[DCE]_{inlet}$ = 25 ppmv, [DMPO] = 100 mM, $[H_2O_2]_0$ = 40 mM, catalyst dosage = 0.2 g/L, pH 3.0.

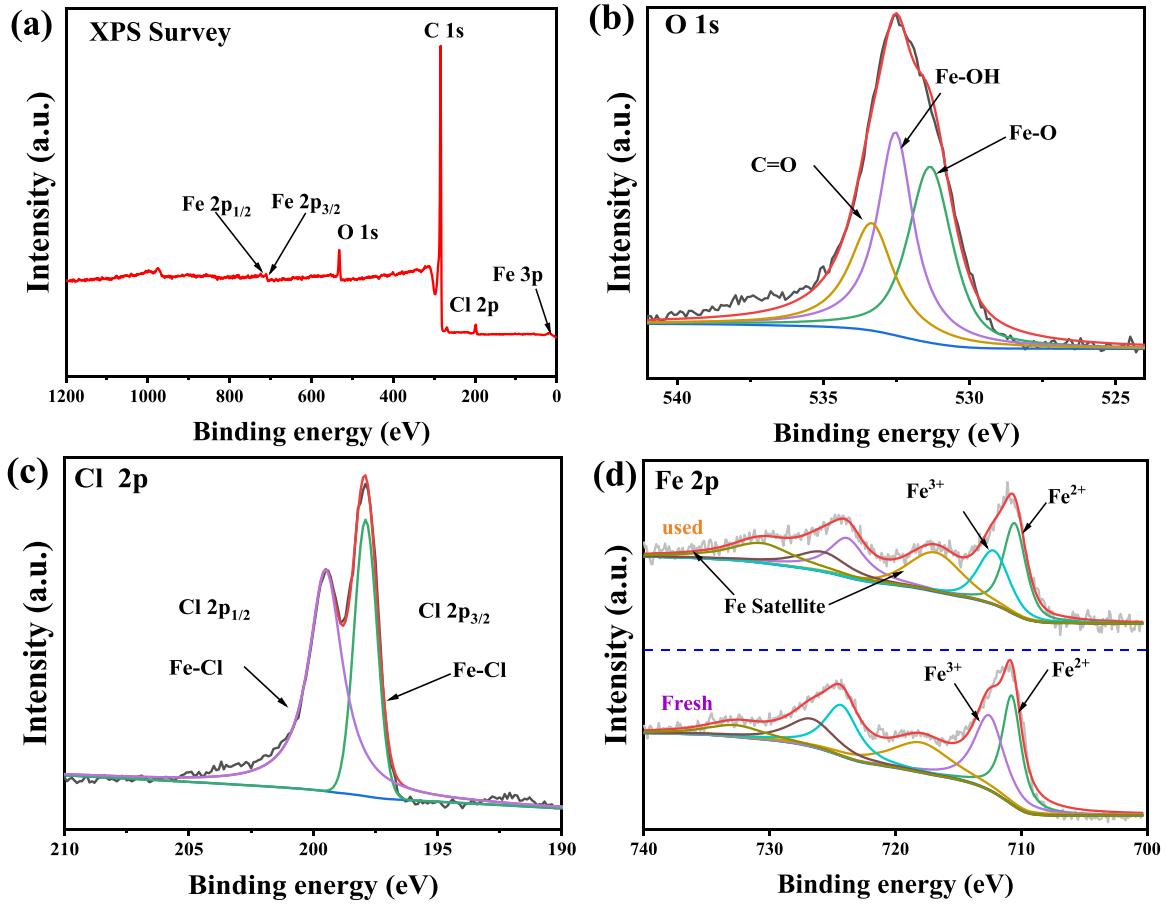

Fig. 5. (a) XPS survey scan for a FeOCl/PGC4, high resolution XPS of (b) O 1 s, (c) Cl 2p and (d) Fe 2p of the FeOCl/PGC4.

increased to 1.08 after the wet scrubbing process. The increase in the surface Fe^{2+} content after the reaction confirmed that the surface Fe^{3+} in FeOCl/H_2O_2 system was reduced to Fe^{2+}. The Fe^{2+}/Fe^{3+} cycle was beneficial toward the continuous activation of H_2O_2 to generate $HO^{\bullet}$.

The possible mechanism for the wet scrubbing of gaseous organics using the FeOCl/PGC+H_2O_2 system is proposed and illustrated in Fig. 6. The dissolved organic molecules readily undergo intra-particle diffusion via the mesoporous channels and are then adsorbed on the carbon surface, which promotes the continuous transfer of gaseous DCE into water. Meanwhile, the surface Fe^{3+} species on FeOCl particle are reduced to Fe^{2+} upon reaction with H_2O_2 (Eqs. (9–10)), the transition state ($\equiv Fe^{2+}\bullet O_2H$) further decomposes into surface Fe^{2+} and $HO_2^{\bullet}$ [49]. The resultant surface Fe^{2+} species activate H_2O_2 to generate $HO^{\bullet}$ (Eq. (11)) [44]. The adsorbed DCE readily diffuses through the mesopores to access and consume the $HO^{\bullet}$ to form soluble intermediates or mineralized products. H_2O_2 participates in the Fe^{2+}/Fe^{3+} cycle (Eq. (11)).

$$\equiv Fe^{3+} + H_2O_2 \rightarrow \equiv Fe^{3+}\cdot H_2O_2 \rightarrow \equiv Fe^{2+}\bullet O_2H + H^+ \quad (9)$$

$$\equiv Fe^{2+}\bullet O_2H \rightarrow \equiv Fe^{2+} + HO_2^{\bullet} \quad (10)$$

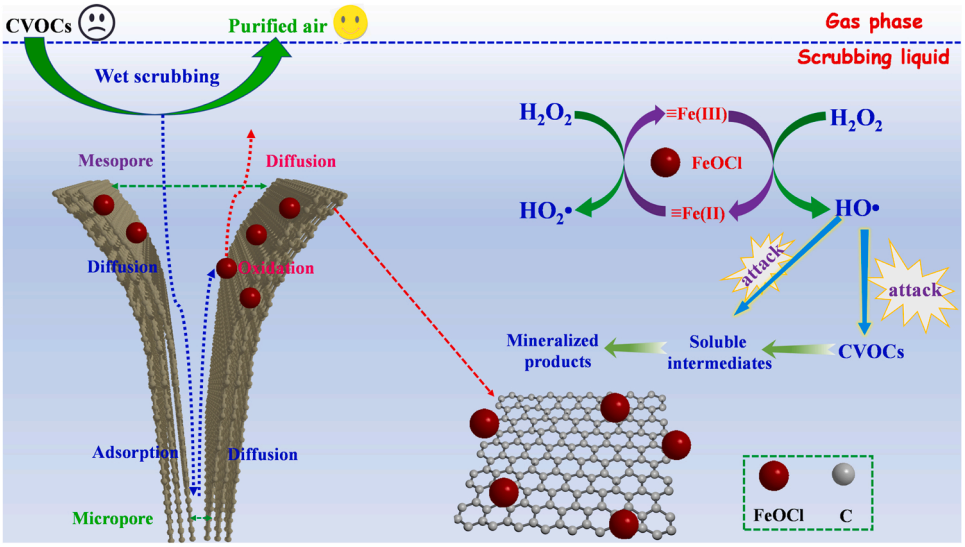

Fig. 6. A scheme illustrating the mechanism for the wet scrubbing of CVOCs in the FeOCl/PGC+H_2O_2 system.

$$\equiv Fe^{2+} + H_2O_2 \rightarrow \equiv Fe^{3+} + OH^- + HO^{\bullet} \quad (11)$$

3.4. DCE degradation pathway and DFT calculations

IC and GC-MS were used to identify the intermediate products formed during the reaction process in order to reveal the degradation pathway of DCE in the FeOCl/PGC4 +H_2O_2 system. Eight products, including ethylene chlorohydrin, ethylene glycol, glyoxal, vinyl alcohol, acetaldehyde, chloroacetic acid, acetic acid and formic acid were detected, as shown in Table S3 and Fig. S10 and S11. In addition, the Fukui function based on density functional theory (DFT) was calculated using Gaussian16 to elucidate the DCE degradation pathway. Relevant information in regard the DFT calculations is shown in Text S3. The natural population analysis (NPA) charge distribution and Fukui index representing radical attack (f^0) and electrophilic attack (f^-) of the atoms in DCE are displayed in Fig. 7a-b, respectively. In general, the larger Fukui index ranking, the more reactive the molecular site and the more vulnerable it is to attack [58]. For instance, C and Cl atoms with high f^- may be vulnerable to electrophilic attack, while 2(H) and 5(H) atoms with the highest f^+ are more susceptible to nucleophilic attack. Since HO• is a mild electrophile [59], it is expected that the reaction

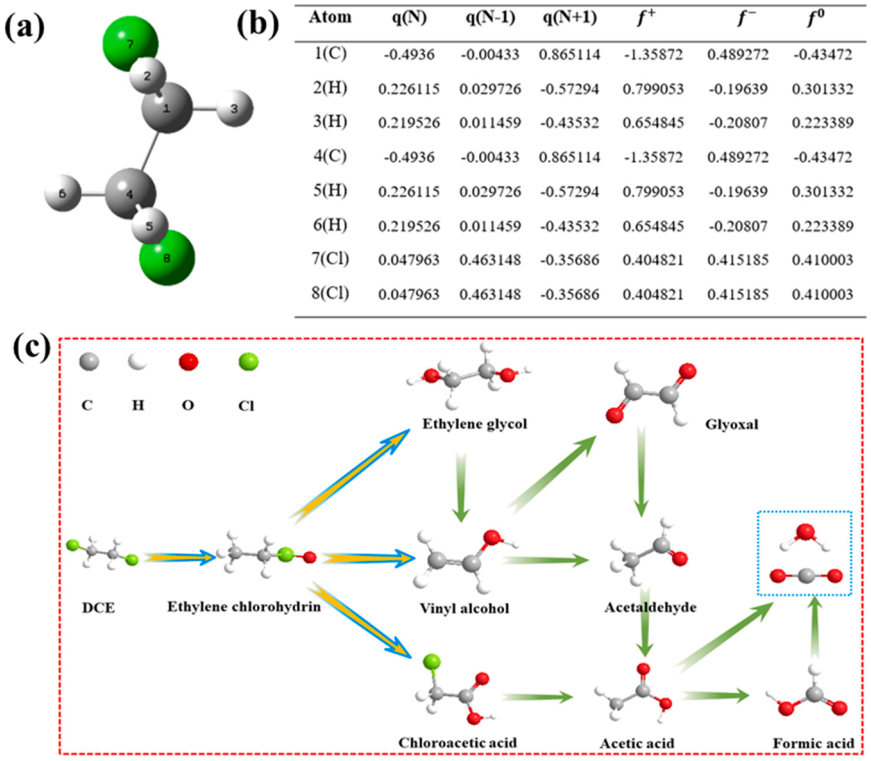

Atom	q(N)	q(N-1)	q(N+1)	f^+	f^-	f^0
1(C)	-0.4936	-0.00433	0.865114	-1.35872	0.489272	-0.43472
2(H)	0.226115	0.029726	-0.57294	0.799053	-0.19639	0.301332
3(H)	0.219526	0.011459	-0.43532	0.654845	-0.20807	0.223389
4(C)	-0.4936	-0.00433	0.865114	-1.35872	0.489272	-0.43472
5(H)	0.226115	0.029726	-0.57294	0.799053	-0.19639	0.301332
6(H)	0.219526	0.011459	-0.43532	0.654845	-0.20807	0.223389
7(Cl)	0.047963	0.463148	-0.35686	0.404821	0.415185	0.410003
8(Cl)	0.047963	0.463148	-0.35686	0.404821	0.415185	0.410003

Fig. 7. (a) DCE chemical structure and (b) NPA change distribution and Fukui index of DCE; (c) proposed DCE degradation pathways in the FeOCl/PGC4 +H_2O_2 system.

between HO• and DCE proceeds via electrophilic attack.

The degradation pathway of DCE in FeOCl/PGC4 +H_2O_2 system is depicted in Fig. 7c. First, a Cl atom on DCE is replaced by a hydroxyl group to generate ethylene chlorohydrin, which was further converted into vinyl alcohol, chloroacetic acid and ethylene glycol via dechlorination [13,23]. In addition, ethylene glycol loses a water molecule via an elimination reaction to form vinyl alcohol, which is then oxidized to an aldehyde or acid. Moreover, the unstable glyoxal is converted into acetaldehyde, which was then further oxidized into small organic compounds, such as acetic acid and formic acid, and then further mineralized to generate CO_2 and H_2O [60,61]. In summary, our DFT calculations were consistent with the GC-MS and IC analyzes, suggesting that the proposed degradation pathway of DCE is feasible.

The concentrations of chloroacetic acid, acetic acid and formic acid were monitored by IC and their variation during the scrubbing process is shown in Fig. S10. This demonstrates that these acids accumulate in the solution over time. The intermediates are water-soluble and their competition with DCE for adsorption sites on the carbon surface was a disadvantage. Therefore, they diffuse into the bulk solution with less probability of consuming the HO• generated on the catalytic sites, resulting in their accumulation in the scrubbing solution.

3.5. Influencing factors

3.5.1. Influence of pH

The DCE removal efficiency in the FeOCl/PGC4 +H_2O_2 system at pH 3–7 is shown in Fig. 8a. The best DCE removal was achieved at pH 3 with 89.1% removal observed after 500 min. The DCE removal efficiency decreased with increasing pH. At an increased pH, hydrous Fe^{3+} originating from the dissolution of FeOCl is more likely to form hydroxide (Eq. (4)), which may deposit on the catalyst and reconstruct the catalyst surface. In addition, previous work suggested that self-decomposition of H_2O_2 as well as passivation of catalyst surface would occur at higher pH [62].

The pH-dependence of the DCE removal efficiency was consistent with the ESR intensity of the DMPO-HO• adducts observed under the different pH conditions studied (Fig. S12a). Our results suggest that pH 3.0 was optimal for the FeOCl/PGC4 +H_2O_2 system. In addition, we monitored the pH of the system over time during wet scrubbing operating at pH 3 and the results showed that the pH remained stable throughout the test period (Fig. S13).

3.5.2. Influence of the catalyst dosage

Fig. 8b shows the influence of the catalyst dosage on the removal of DCE. The best DCE removal was obtained at a catalyst dosage of 0.2 g/L. At higher catalyst dosages, more adsorption sites are available for DCE adsorption and more catalytic sites are available for H_2O_2 activation. However, excess Fe will seriously accelerate the consumption of HO• (Eq. (12)) [43], which will induce an adverse effect on the DCE oxidation process. As a result, further increasing the catalyst dosage actually reduces the efficiency of the system. This was confirmed by the ESR spectra obtained after 300 min, which revealed that the most intensive ESR signal of the DMPO-HO• adduct was observed at a catalyst dosage of 0.2 g/L (Fig. S12b).

$$HO^{\bullet} + \equiv Fe^{2+} \rightarrow OH^{-} + \equiv Fe^{3+} \quad (12)$$

3.5.3. Influence of the H_2O_2 concentration

The effect of the H_2O_2 concentration on the removal of DCE in the FeOCl/PGC4 +H_2O_2 system is shown in Fig. 8c. The DCE removal efficiency gradually increases upon gradually increasing $[H_2O_2]_0$ from 10 to 40 mM, whereas further increasing $[H_2O_2]_0$ to 50 mM reduced the DCE removal rate. Excessive H_2O_2 can scavenge the HO• produced (Eq. (13)).

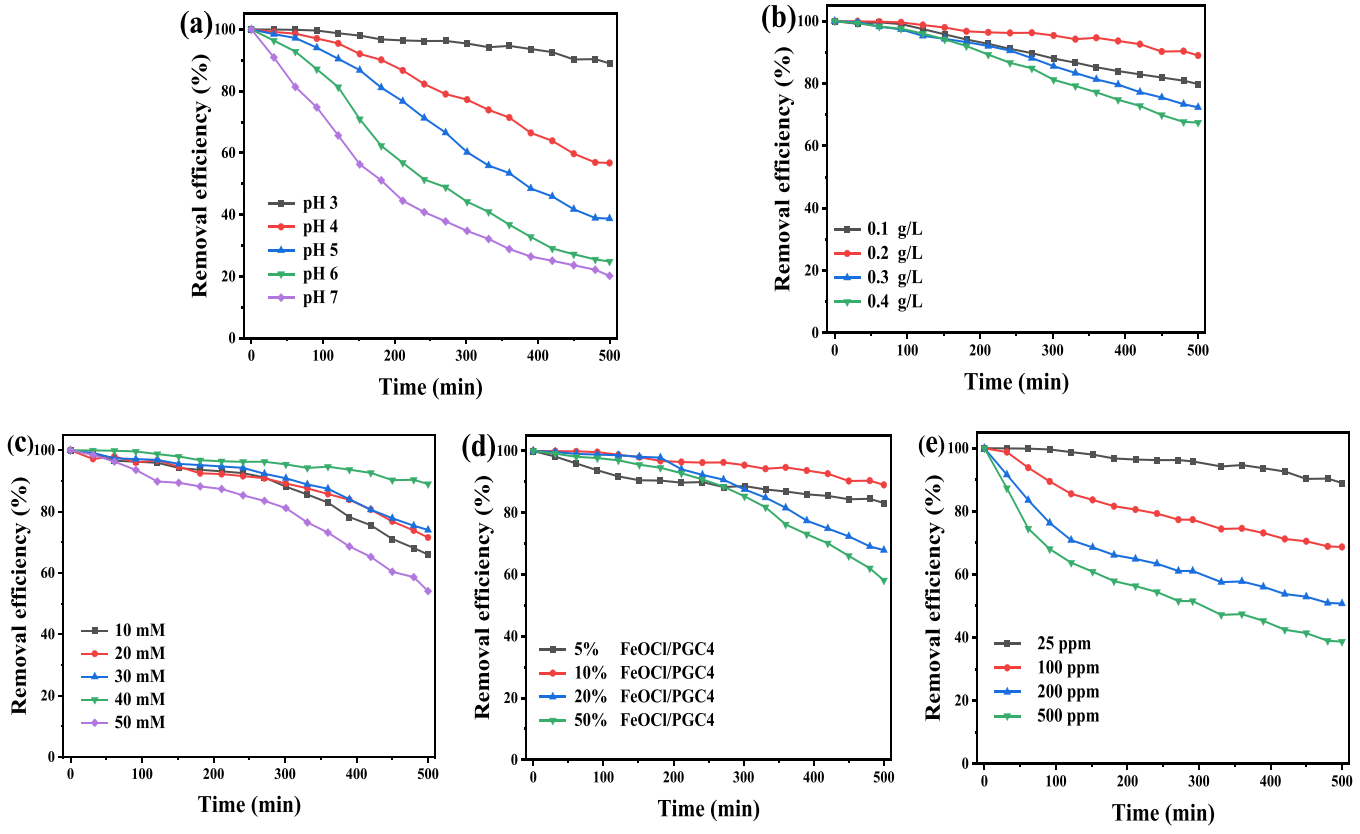

Fig. 8. Effect of (a) pH, (b) FeOCl/PGC4 dosage, (c) H_2O_2 dosage, (d) FeOCl loadings and (e) inlet DCE concentration on the DCE removal efficiency. Reaction conditions: $[DCE]_{inlet}$ = 25 ppmv, catalyst dosage = 0.2 g/L, $[H_2O_2]_0$ = 40 mM, pH 3.0.

The ESR spectra obtained for the systems with various $[H_2O_2]_0$ after 300 min also demonstrate that the strongest ESR signal of the DMPO-HO$^\bullet$ adduct was observed at $[H_2O_2]_0 = 40$ mM (Fig. S12c), which was in good agreement with the DCE removal efficiency.

$$H_2O_2 + HO^\bullet \rightarrow H_2O + {}^\bullet O_2H \quad (13)$$

3.5.4. Influence of the FeOCl loading

The effect of the FeOCl loading on the removal of DCE is shown in Fig. 8d. The most efficient DCE removal was achieved at a FeOCl loading of 10%. Further increasing the loading actually decreases the DCE removal efficiency although it could increase the number of catalytic sites available. Furthermore, ESR experiments also revealed that further increasing the FeOCl loading to > 10% reduced the signal intensity of the DMPO-HO$^\bullet$ adduct observed after 300 min (Fig. S12d). A plausible explanation is that higher loadings have enhanced HO$^\bullet$ quenching effects (Eqs. (12) and (14))[43].

$$\equiv Fe^{3+} + H_2O_2 \rightarrow \equiv Fe^{2+}\bullet O_2H + H^+ \quad (14)$$

3.5.5. Influence of the DCE concentration

Fig. 8e displays the removal curves obtained for gaseous DCE at different concentrations. The removal efficiency decreased with an increase in the DCE concentration. This could be attributed to the number of adsorbent sites and catalytic sites becoming insufficient at high DCE concentrations leading to the decrease in the removal rate. Therefore, increasing the FeOCl/PGC4 dosage to promote the removal of high concentrations of DCE may be a feasible strategy, as discussed below.

3.6. Long-term DCE removal

The removal rate of 25 ppmv DCE in the FeOCl/PGC4 +H_2O_2 system begins to decline after 300 min (Fig. 2a), which was due to the consumption of H_2O_2. Therefore, H_2O_2 should be supplemented for the long-term efficient and continuous removal of DCE. We tried supplementing H_2O_2 by pulsed dosing and continuous dosing.

During wet scrubbing of 25 ppmv DCE at a FeOCl/PGC4 dosage of 0.2 g/L, 10 mM H_2O_2 was added to start the AOPs, and then added every 300 min. The DCE removal rate curve and changes in the H_2O_2 concentration are shown in Fig. 9a. The DCE removal rate remains at a high level throughout the 1200 min process and a removal rate of 89.2% was still observed at the end of the process. Meanwhile, the concentration of H_2O_2 in the wet scrubbing solution was between 0.11 and 11.6 mM during the whole process. This indicates that DCE could be stably removed within this H_2O_2 concentration range achieved via pulsed dosing.

During wet scrubbing of 200 ppmv DCE at an enhanced FeOCl/PGC4 dosage of 0.6 g/L with H_2O_2 continuously added at a rate of 3 mM/h, a DCE removal rate of > 85% was maintained over 600 min (Fig. 9b) and the concentration of H_2O_2 in the wet scrubbing solution was < 4 mM during the process. This indicates that the stable removal of DCE can be achieved at low H_2O_2 concentrations. For comparison, we tested the DCE removal efficiencies in one-time dosing mode (30 mM H_2O_2 added at the beginning) and pulsed dosing mode (5 mM H_2O_2 added every 100 min). The DCE removal curves obtained using the different modes were compared in Fig. S14. It shows that the continuous dosing mode was superior to the other two modes in dealing with 200 ppmv DCE. The higher adsorbent/catalyst dosage facilitates the removal of high concentrations of VOCs. However, it inevitably accelerates the decomposition of H_2O_2 and thus leads to the waste of reagents. In continuous dosing mode, H_2O_2 can be maintained at a low, but sufficiently functional concentration range.

3.7. Stability and practical application of FeOCl/PGC4

Five consecutive DCE degradation experiments were performed to evaluate the reusability of FeOCl/PGC4. After each 500-min wet scrubbing process (working process), H_2O_2 (40 mM) was added to the scrubbing liquid without removing the catalyst and stirred under nitrogen to further oxidize the intermediates (regeneration process), prior to the next working process. Fig. 10a shows the DCE removal curves obtained for the cycling experiments. At the end of the fifth cycle of the test, the system still achieved a DCE removal rate of about 70%, indicating that FeOCl/PGC exhibits good catalytic activity for a long time. The total organic carbon (TOC) in the scrubbing liquid was measured and the TOC evolution is shown in Fig. 10b. During each working process, the TOC gradually increases, indicating the accumulation of organic molecules in the solution. The TOC at the end of the first working process was 0.78 mg/L, while the total carbon captured from the gas flow by the scrubbing solution, calculated from the DCE removal curve, was 1.30 mg/L, indicating that more than half of the organic carbon was not mineralized during working process. After each regeneration process, the TOC decreased by about 90% and the residual TOC before starting the next working process was low. This indicates although soluble intermediates are difficult to oxidize in time by HO$^\bullet$ generated on the catalyst under a continuous DCE feed, they can be further oxidized and mineralized via a catalytic peroxide oxidation post-treatment step. Complete mineralization is possible by further optimizing the regeneration conditions, for example, by increasing the H_2O_2 concentration. In practical applications, such a strategy can be adopted

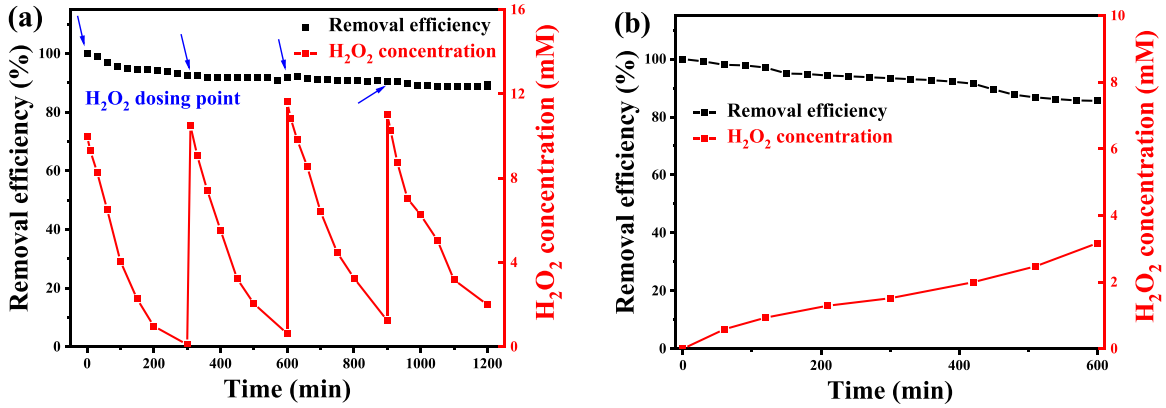

Fig. 9. (a) Removal of low-concentration DCE in pulsed H_2O_2 dosing mode. Reaction conditions: $[DCE]_{inlet} = 25$ ppmv, catalyst dosage = 0.2 g/L, pH 3.0. (b) Removal of high-concentration DCE in continuous H_2O_2 dosing mode. Reaction conditions: $[DCE]_{inlet} = 200$ ppmv, catalyst dosage = 0.6 g/L, H_2O_2 dosing rate = 3 mM/h, pH 3.0.

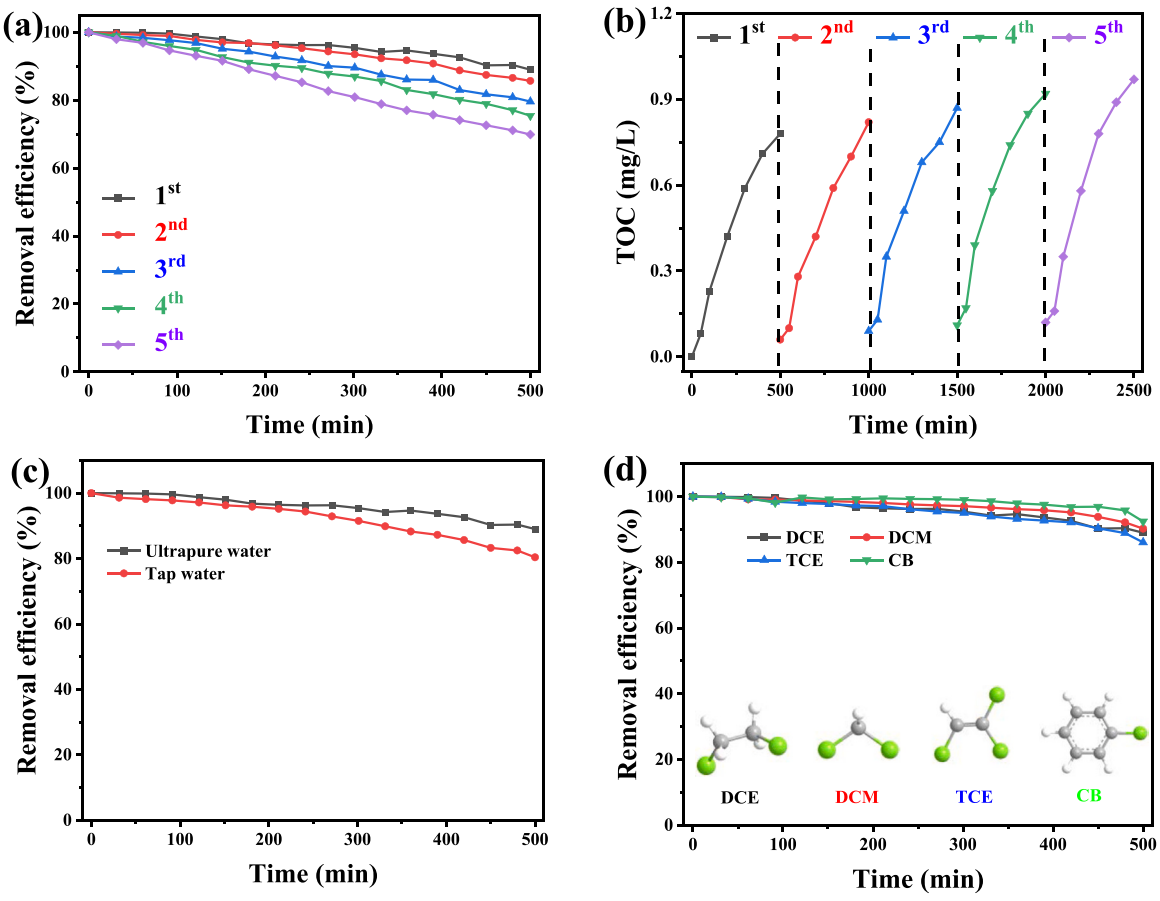

Fig. 10. (a) Degradation of DCE in 500 min by the regenerated scrubbing system, (b) variation of TOC with time during cycling working process (c) effect of tap water on DCE removal and (d) degradation of different CVOCs in the FeOCl/PGC4 +H_2O_2 system. Reaction conditions: $[DCE]_{inlet}$ = 25 ppmv, $[H_2O_2]_0$ = 40 mM, catalyst dosage = 0.2 g/L, pH 3.0.

to regenerate the scrubbing system during non-working hours. We determined the concentration of dissolved Fe present in the solution. The amount of leached Fe ions increases with time in the first working process (Fig. S15a) and the increase in Fe dissolution gradually slowed down in the subsequent runs (Fig. S15b), implying a gradual establishment of equilibrium between the hydrated Fe ions and solids. The total Fe concentration in the solution after the first working process and after five working processes were 0.65 and 1.67 mg/L, respectively, corresponding to 3.51% and 9.03% of the total Fe in the catalyst, respectively. Nevertheless, the XRD pattern, Raman spectrum and FT-IR spectrum of the used catalyst were almost identical to those of the fresh one (Fig. S16a-c), and the SEM images reveal that the morphology of the catalyst also did not change significance after use (Fig. S17), indicating that the catalyst was somewhat stable. In addition, we built wet scrubbers coupled with a homogeneous Fenton process using 0.65 and 1.67 mg/L Fe^{2+}, which gave DCE removal curves almost identical to that obtained for the pure water system (Fig. S18), suggesting that the contribution from the homogeneous Fenton process to the removal of gaseous DCE was negligible at very low concentrations of Fe^{2+} and dissolved DCE in the bulk solution.

We also prepared a scrubbing solution comprised of FeOCl/PGC4 +H_2O_2 using tap water and the DCE removal curve obtained for this system is shown in Fig. 10c. It demonstrated that the DCE removal in this system was > 80% for 500 min, suggesting that tap water is also applicable for the preparation of the scrubbing solution.

The wet scrubbing of other gaseous CVOCs (25 ppm), including DCM, TCE and CB, were also studied (Fig. 10d). The FeOCl/PGC4 +H_2O_2 system achieved more than 89.1%, 90.3%, 86.1% and 92.4% removal of DCE, DCM, TCE and CB, respectively within 500 min. This implies that the wet scrubbing system is effective for various recalcitrant CVOCs.

4. Conclusions

FeOCl catalyst supported on PGC has been successfully prepared using a facile thermal conversion of impregnated $FeCl_3$•6 H_2O at 150 °C. In the wet scrubbing process, FeOCl/PGC activated H_2O_2 to produce $HO^•$, which effectively degraded CVOCs. The wet scrubber can treat gaseous DCE, DCM, TCE and CB with removal rates of > 80% over 500 min. When compared with microporous activated carbon, PGC with well-developed mesopores facilitated the intra-particle diffusion of organic molecules and thus, exhibited better performance. With pulsed or continuous H_2O_2 dosing, the FeOCl/PGC4 +H_2O_2 system at pH 3 achieved long-term dichloroethane removal (>85%). Tap water was used as an alternative to pure water for the preparation of the scrubbing solution without causing obvious loss of efficiency. The study demonstrates that the FeOCl/PGC4 +H_2O_2 system is promising for the treatment of organic waste gases.

CRediT authorship contribution statement

Cong Pan: Investigation, Formal analysis, Writing – original draft. **Wenyu Wang**: Investigation, Writing – original draft. **Yihui Zhang**: Software. **Jong Chol Nam**: Validation. **Zhixiong You**: Methodology. **Feng Wu**: Project administration, Formal analysis. **Jing Xu**: Funding acquisition, Writing – review & editing. **Jinjun Li**: Conceptualization, Supervision, Project administration, Funding acquisition.

Declaration of Competing Interest

The authors declare that they have no known competing financial interests or personal relationships that could have appeared to influence the work reported in this paper.

Data Availability

Data will be made available on request.

Acknowledgments

This work was supported by the National Natural Science Foundation of China (21876137 and 22061132001).

Appendix A. Supporting information

Supplementary data associated with this article can be found in the online version at doi:10.1016/j.apcatb.2023.122659.

References

[1] X. Feng, M. Tian, C. He, L. Li, J.-W. Shi, Y. Yu, J. Cheng, Yolk-shell-like mesoporous CoCrOx with superior activity and chlorine resistance in dichloromethane destruction, Appl. Catal. B Environ. 264 (2020), 118493, https://doi.org/10.1016/j.apcatb.2019.118493.

[2] F.R. Dalby, S. Svane, J.J. Sigurdarson, M.K. Sørensen, M.J. Hansen, H. Karring, A. Feilberg, Synergistic tannic acid-fluoride inhibition of ammonia emissions and simultaneous reduction of methane and odor emissions from livestock waste, Environ. Sci. Technol. 54 (2020) 7639–7650, https://doi.org/10.1021/acs.est.0c01231.

[3] N. Li, X. Xing, J. Cheng, Z. Zhang, Z. Hao, Influence of oxygen and water content on the formation of polychlorinated organic by-products from catalytic degradation of 1,2-dichlorobenzene over a Pd/ZSM-5 catalyst, J. Hazard. Mater. 403 (2021), 123952, https://doi.org/10.1016/j.jhazmat.2020.123952.

[4] M.F. Mustafa, Y. Liu, Z. Duan, H. Guo, S. Xu, H. Wang, W. Lu, Volatile compounds emission and health risk assessment during composting of organic fraction of municipal solid waste, J. Hazard. Mater. 327 (2017) 35–43, https://doi.org/10.1016/j.jhazmat.2016.11.046.

[5] J. Yoon, S.K. Chae, J.M. Kim, Colorimetric sensors for volatile organic compounds (VOCs) based on conjugated polymer-embedded electrospun fibers, J. Am. Chem. Soc. 129 (2007) 3038–3039, https://doi.org/10.1021/ja067856+.

[6] Y. Cheng, J. Jiang, L. Xia, H. Xu, C. Ye, J. Sun, R. Gu, Investigation and accounting research of VOC in daily and specialty ceramic industry, Coatings 12 (2022) 1–16, https://doi.org/10.3390/coatings12020279.

[7] M. Kampa, E. Castanas, Human health effects of air pollution, Environ. Pollut. 151 (2008) 362–367, https://doi.org/10.1016/j.envpol.2007.06.012.

[8] Z. Su, W. Yang, C. Wang, S. Xiong, X. Cao, Y. Peng, W. Si, Y. Weng, M. Xue, J. Li, Roles of oxygen vacancies in the bulk and surface of CeO_2 for toluene catalytic combustion, Environ. Sci. Technol. 54 (2020) 12684–12692, https://doi.org/10.1021/acs.est.0c03981.

[9] X. Liu, L. Chen, T. Zhu, R. Ning, Catalytic oxidation of chlorobenzene over noble metals (Pd, Pt, Ru, Rh) and the distributions of polychlorinated by-products, J. Hazard. Mater. 363 (2019) 90–98, https://doi.org/10.1016/j.jhazmat.2018.09.074.

[10] P. Chen, L. Chen, X. Dong, H. Wang, J. Li, Y. Zhou, C. Xue, Y. Zhang, F. Dong, Enhanced photocatalytic VOCs mineralization via special Ga-O-H charge transfer channel in α-Ga_2O_3/MgAl-LDH heterojunction, ACS EST Eng. 1 (2021) 501–511, https://doi.org/10.1021/acsestengg.0c00194.

[11] C. He, J. Cheng, X. Zhang, M. Douthwaite, S. Pattisson, Z. Hao, Recent advances in the catalytic oxidation of volatile organic compounds: A review based on pollutant sorts and sources, Chem. Rev. 119 (2019) 4471–4568, https://doi.org/10.1021/acs.chemrev.8b00408.

[12] L. Zhu, D. Shen, K.H. Luo, A critical review on VOCs adsorption by different porous materials: Species, mechanisms and modification methods, J. Hazard. Mater. 389 (2020), 122102, https://doi.org/10.1016/j.jhazmat.2020.122102.

[13] H. Wang, H. Guo, Y. Zhao, X. Dong, M. Gong, Thermodynamic analysis of a petroleum volatile organic compounds (VOCs) condensation recovery system combined with mixed-refrigerant refrigeration, Int. J. Refrig. 116 (2020) 23–35, https://doi.org/10.1016/j.ijrefrig.2020.03.011.

[14] P.F. Biard, A. Couvert, C. Renner, J.P. Levasseur, Intensification of volatile organic compounds mass transfer in a compact scrubber using the O_3/H_2O_2 advanced oxidation process: Kinetic study and hydroxyl radical tracking, Chemosphere 85 (2011) 1122–1129, https://doi.org/10.1016/j.chemosphere.2011.07.050.

[15] C. Domeno, A. Rodríguez-Lafuente, J.M. Martos, R. Bilbao, C. Nerín, VOC removal and deodorization of effluent gases from an industrial plant by photo-oxidation, chemical oxidation, and ozonization, Environ. Sci. Technol. 44 (2010) 2585–2591, https://doi.org/10.1021/es902735g.

[16] X. Xie, R. Xie, Z. Suo, H. Huang, M. Xing, D. Lei, A highly dispersed Co-Fe bimetallic catalyst to activate peroxymonosulfate for VOC degradation in a wet scrubber, Environ. Sci. Nano 8 (2021) 2976–2987, https://doi.org/10.1039/d1en00547b.

[17] R. Xie, J. Ji, H. Huang, D. Lei, R. Fang, Y. Shu, Y. Zhan, K. Guo, D.Y.C. Leung, Heterogeneous activation of peroxymonosulfate over monodispersed Co_3O_4/activated carbon for efficient degradation of gaseous toluene, Chem. Eng. J. 341 (2018) 383–391, https://doi.org/10.1016/j.cej.2018.02.045.

[18] R. Xie, J. Cao, X. Xie, D. Lei, K. Guo, H. Liu, Y. Zeng, H. Huang, Mechanistic insights into complete oxidation of chlorobenzene to CO_2 via wet scrubber coupled with UV/PDS, Chem. Eng. J. 401 (2020), 126077, https://doi.org/10.1016/j.cej.2020.126077.

[19] G. Liu, J. Ji, H. Huang, R. Xie, Q. Feng, Y. Shu, Y. Zhan, R. Fang, M. He, S. Liu, X. Ye, D.Y.C. Leung, UV/H_2O_2: An efficient aqueous advanced oxidation process for VOCs removal, Chem. Eng. J. 324 (2017) 44–50, https://doi.org/10.1016/j.cej.2017.04.105.

[20] Z. Cheng, J. Wang, D. Chen, J. Chen, L. Wang, J. Ye, J. Yu, Thermally activated persulfate for gaseous p-xylene removal: Process optimization, mechanism investigation, and pathway analysis, Chem. Eng. J. 421 (2021), 127728, https://doi.org/10.1016/j.cej.2020.127728.

[21] X. Lai, X. Ning, J. Chen, Y. Li, Y. Zhang, Y. Yuan, Comparison of the Fe^{2+}/H_2O_2 and Fe^{2+}/PMS systems in simulated sludge: Removal of PAHs, migration of elements and formation of chlorination by-products, J. Hazard. Mater. 398 (2020), 122826, https://doi.org/10.1016/j.jhazmat.2020.122826.

[22] G. Nie, K. Hu, W. Ren, P. Zhou, X. Duan, L. Xiao, S. Wang, Mechanical agitation accelerated ultrasonication for wastewater treatment: Sustainable production of hydroxyl radicals, Water Res 198 (2021), 117124, https://doi.org/10.1016/j.watres.2021.117124.

[23] W.G. Jeong, J.G. Kim, K. Baek, Removal of 1,2-dichloroethane in groundwater using Fenton oxidation, J. Hazard. Mater. 428 (2022), 128253, https://doi.org/10.1016/j.jhazmat.2022.128253.

[24] Y. Shen, S. Zhao, Y. Lu, J. Yang, J. Wang, S. Zhang, Effective degradation of VOCs from wood by Fe^{2+} chelate activated dual oxidant (H_2O_2-PS, Chemosphere 291 (2022), 132882, https://doi.org/10.1016/j.chemosphere.2021.132882.

[25] X. Zhang, Y. Ding, H. Tang, X. Han, L. Zhu, N. Wang, Degradation of bisphenol A by hydrogen peroxide activated with $CuFeO_2$ microparticles as a heterogeneous Fenton-like catalyst: efficiency, stability and mechanism, Chem. Eng. J. 236 (2014) 251–262, https://doi.org/10.1016/j.cej.2013.09.051.

[26] A. Babuponnusami, K. Muthukumar, Removal of phenol by heterogenous photo electro Fenton-like process using nano-zero valent iron, Sep. Purif. Technol. 98 (2012) 130–135, https://doi.org/10.1016/j.seppur.2012.04.034.

[27] S. Zhang, X. Zhao, H. Niu, Y. Shi, Y. Cai, G. Jiang, Superparamagnetic Fe_3O_4 nanoparticles as catalysts for the catalytic oxidation of phenolic and aniline compounds, J. Hazard. Mater. 167 (2009) 560–566, https://doi.org/10.1016/j.jhazmat.2009.01.024.

[28] Y. Wang, R. Wang, N. Lin, Y. Wang, X. Zhang, Highly efficient microwave-assisted Fenton degradation bisphenol A using iron oxide modified double perovskite intercalated montmorillonite composite nanomaterial as catalyst, J. Colloid Interface Sci. 594 (2021) 446–459, https://doi.org/10.1016/j.jcis.2021.03.046.

[29] H. Sun, G. Xie, D. He, L. Zhang, Ascorbic acid promoted magnetite Fenton degradation of alachlor: Mechanistic insights and kinetic modeling, Appl. Catal. B Environ. 267 (2020), 118383, https://doi.org/10.1016/j.apcatb.2019.118383.

[30] X. Hou, X. Huang, F. Jia, Z. Ai, J. Zhao, L. Zhang, Hydroxylamine promoted goethite surface Fenton degradation of prganic pollutants, Environ. Sci. Technol. 51 (2017) 5118–5126, https://doi.org/10.1021/acs.est.6b05906.

[31] X.J. Yang, X.M. Xu, J. Xu, Y.F. Han, Iron oxychloride (FeOCl): An efficient Fenton-like catalyst for producing hydroxyl radicals in degradation of organic contaminants, J. Am. Chem. Soc. 135 (2013) 16058–16061, https://doi.org/10.1021/ja409130c.

[32] J. Zhang, G. Zhang, Q. Ji, H. Lan, J. Qu, H. Liu, Carbon nanodot-modified FeOCl for photo-assisted Fenton reaction featuring synergistic in-situ H_2O_2 production and activation, Appl. Catal. B Environ. 266 (2020), 118665, https://doi.org/10.1016/j.apcatb.2020.118665.

[33] Z. Li, C. Shen, Y. Liu, C. Ma, F. Li, B. Yang, M. Huang, Z. Wang, L. Dong, S. Wolfgang, Carbon nanotube filter functionalized with iron oxychloride for flow-through electro-Fenton, Appl. Catal. B Environ. 260 (2020), 118204, https://doi.org/10.1016/j.apcatb.2019.118204.

[34] M. Sun, C. Chu, F. Geng, X. Lu, J. Qu, J. Crittenden, M. Elimelech, J.H. Kim, Reinventing Fenton chemistry: Iron oxychloride nanosheet for pH-insensitive H_2O_2 activation, Environ. Sci. Technol. Lett. 5 (2018) 186–191, https://doi.org/10.1021/acs.estlett.8b00065.

[35] C. Fu, C. Pan, T. Chen, D. Peng, Y. Liu, F. Wu, J. Xu, Z. You, J. Li, L. Luo, Adsorption-enforced Fenton-like process using activated carbon-supported iron oxychloride catalyst for wet scrubbing of airborne dichloroethane, Chemosphere 307 (2022), 136193, https://doi.org/10.1016/j.chemosphere.2022.136193.

[36] L. Hu, Y. Peng, F. Wu, S. Peng, J. Li, Z. Liu, Tubular activated carbons made from cotton stalk for dynamic adsorption of airborne toluene, J. Taiwan Inst. Chem. Eng. 80 (2017) 399–405, https://doi.org/10.1016/j.jtice.2017.07.029.

[37] L. Hu, W. Cheng, W. Zhang, F. Wu, S. Peng, J. Li, Monolithic bamboo-based activated carbons for dynamic adsorption of toluene, J. Porous Mater. 24 (2017) 541–549, https://doi.org/10.1007/s10934-016-0289-6.

[38] T. Chen, C. Fu, Y. Liu, F. Pan, F. Wu, Z. You, J. Li, Adsorption of volatile organic compounds by mesoporous graphitized carbon: Enhanced organophilicity, humidity resistance, and mass transfer, Sep. Purif. Technol. 264 (2021), 118464, https://doi.org/10.1016/j.seppur.2021.118464.

[39] F. Pan, T. Chen, M. Cai, F. Wu, Z. You, J. Li, Fabrication of large-surface-area graphitized carbons by potassium hydroxide-promoted catalytic graphitization, Mater. Res. Bull. 140 (2021), 111333, https://doi.org/10.1016/j.materresbull.2021.111333.
[40] M. Yan, Y. Rong, F. Wu, Z. You, D. Wang, X. Yang, Z. Hao, J. Li, Z. Zhang, Micro-mesoporous graphitized carbon fiber as hydrophobic adsorbent that removes volatile organic compounds from air, Chem. Eng. J. 452 (2023), 139184, https://doi.org/10.1016/j.cej.2022.139184.
[41] J. Zhang, G. Liu, S. Liu, 2D/2D FeOCl/graphite oxide heterojunction with enhanced catalytic performance as a photo-Fenton catalyst, N. J. Chem. 42 (2018) 6896–6902, https://doi.org/10.1039/c8nj00647d.
[42] H. Afşar, R. Apak, I. Tor, Spectrophotometric determination of hydrogen peroxide using tris(1,10-phenanthroline)iron(II, Analyst 115 (1990) 99–103, https://doi.org/10.1039/AN9901500099.
[43] C. Pan, L. Fu, F. Lide, Y. Ding, C. Wang, J. Huang, S. Wang, Insights into bromate reduction by Fe(II): Multiple radicals generation and carbamazepine oxidation, Chem. Eng. J. 431 (2022), 133957, https://doi.org/10.1016/j.cej.2021.133957.
[44] Y. Cao, K. Cui, Y. Chen, M. Cui, G. Li, D. Li, X. Yang, Efficient degradation of tetracycline by H_2O_2 catalyzed by FeOCl: A wide range of pH values from 3 to 7, Solid State Sci. 113 (2021), 106548, https://doi.org/10.1016/j.solidstatesciences.2021.106548.
[45] M. Thommes, K. Kaneko, A.V. Neimark, J.P. Olivier, F. Rodriguez-reinoso, J. Rouquerol, K.S.W. Sing, Physisorption gases, Spec. Ref. Eval. Surf. Area pore size Distrib. (IUPAC Tech. Rep.) 87 (2015) 1051–1069, https://doi.org/10.1515/pac-2014-1117.
[46] J. Dewulf, D. Drijvers, H. Van Langenhove, Measurement of Henry's law constant as function of temperature and salinity for the low temperature range, Atmos. Environ. 29 (1995) 323–331, https://doi.org/10.1016/1352-2310(94)00256-K.
[47] F.C. Wu, R.L. Tseng, R.S. Juang, Initial behavior of intraparticle diffusion model used in the description of adsorption kinetics, Chem. Eng. J. 153 (2009) 1–8, https://doi.org/10.1016/j.cej.2009.04.042.
[48] J. Wang, X. Guo, Rethinking of the intraparticle diffusion adsorption kinetics model: Interpretation, solving methods and applications, Chemosphere 309 (2022), 136732, https://doi.org/10.1016/j.chemosphere.2022.136732.
[49] X. Tian, Y. Chen, Y. Chen, D. Chen, Q. Wang, X. Li, Removal of gaseous hydrogen sulfide by a FeOCl/H_2O_2 wet oxidation system, ACS Omega 7 (2022) 8163–8173, https://doi.org/10.1021/acsomega.2c00267.
[50] Q. Yi, J. Ji, B. Shen, C. Dong, J. Liu, J. Zhang, M. Xing, Singlet oxygen triggered by superoxide radicals in a molybdenum cocatalytic Fenton reaction with rnhanced redox activity in the environment, Environ. Sci. Technol. 53 (2019) 9725–9733, https://doi.org/10.1021/acs.est.9b01676.
[51] X. Liu, C. Wang, T. Zhu, Q. Lv, D. Che, Simultaneous removal of SO_2 and NO with OH from the catalytic decomposition of H_2O_2 over Fe-Mo mixed oxides, J. Hazard. Mater. 404 (2021), 123936, https://doi.org/10.1016/j.jhazmat.2020.123936.
[52] Z. Wang, J. Jiang, S. Pang, Y. Zhou, C. Guan, Y. Gao, J. Li, Y. Yang, W. Qiu, C. Jiang, Is sulfate radical really generated from peroxydisulfate activated by Iron (II) for environmental decontamination? Environ. Sci. Technol. 52 (2018) 11276–11284, https://doi.org/10.1021/acs.est.8b02266.
[53] S. Liang, L. Zhu, J. Hua, W. Duan, P.T. Yang, S.L. Wang, C. Wei, C. Liu, C. Feng, Fe^{2+}/HClO reaction produces $Fe^{IV}O^{2+}$: An enhanced advanced oxidation process, Environ. Sci. Technol. 54 (2020) 6406–6414, https://doi.org/10.1021/acs.est.0c00218.
[54] J. Zou, J. Ma, L. Chen, X. Li, Y. Guan, P. Xie, C. Pan, Rapid acceleration of ferrous iron/peroxymonosulfate oxidation of organic pollutants by promoting Fe(III)/Fe (II) cycle with hydroxylamine, Environ. Sci. Technol. 47 (2013) 11685–11691, https://doi.org/10.1021/es4019145.
[55] J. Zhao, M. Ji, J. Di, Y. Zhang, M. He, H. Li, J. Xia, Novel Z-scheme heterogeneous photo-Fenton-like g-C_3N_4/FeOCl for the pollutants degradation under visible light irradiation, J. Photochem. Photobiol. A Chem. 391 (2020), 112343, https://doi.org/10.1016/j.jphotochem.2019.112343.
[56] C. Tan, Q. Xu, T. Sheng, X. Cui, Z. Wu, H. Gao, H. Li, Reactive oxygen species generation in FeOCl nanosheets activated peroxymonosulfate system: radicals and non-radical pathways, J. Hazard. Mater. 398 (2020), https://doi.org/10.1016/j.jhazmat.2020.123084.
[57] M. Sabri, A. Habibi-Yangjeh, H. Chand, V. Krishnan, Activation of persulfate by novel TiO_2/FeOCl photocatalyst under visible light: Facile synthesis and high photocatalytic performance, Sep. Purif. Technol. 250 (2020), 117268, https://doi.org/10.1016/j.seppur.2020.117268.
[58] C. Zhang, S. Tian, F. Qin, Y. Yu, D. Huang, A. Duan, C. Zhou, Y. Yang, W. Wang, Y. Zhou, H. Luo, Catalyst-free activation of permanganate under visible light irradiation for sulfamethazine degradation: experiments and theoretical calculation, Water Res 194 (2021), 116915, https://doi.org/10.1016/j.watres.2021.116915.
[59] F. De Vleeschouwer, V. Van Speybroeck, M. Waroquier, P. Geerlings, F. De Proft, Electrophilicity and nucleophilicity index for radicals, Org. Lett. 9 (2007) 2720–2724, https://doi.org/10.1021/ol071038k.
[60] Z. Lu, G. Zeng, Z. Zhou, Y. Liu, P. Wang, X. Sheng, J. Dong, A. Idress, Q. Sui, S. Lyu, Effective degradation of 1,2-dichloroethane in calcium peroxide activated by Fe (III): performance and mechanisms, Water Supply 22 (2022) 5589–5602, https://doi.org/10.2166/ws.2022.132.
[61] X. Yu, L. Dai, Y. Peng, J. Deng, Y. Liu, L. Jing, X. Zhang, Z. Hou, J. Wang, H. Dai, High selectivity to HCl for the catalytic removal of 1,2-Dichloroethane over RuP/3DOM WOx: insights into the effects of P-doping and H_2O introduction, Environ. Sci. Technol. 55 (2021) 14906–14916, https://doi.org/10.1021/acs.est.1c05586.
[62] C. Tan, T. Sheng, Q. Xu, T. Xu, K. Sun, L. Deng, W. Xu, Cobalt doped iron oxychloride as efficient heterogeneous Fenton catalyst for degradation of paracetamol and phenacetin, Chemosphere 263 (2021), 127989, https://doi.org/10.1016/j.chemosphere.2020.127989.